Transphosphorylation Catalyzed by Ribonuclease A: Computational Study Using *ab Initio* Effective Fragment Potentials

Brian D. Wladkowski,*,† Morris Krauss, and Walter J. Stevens

Contribution from the Center for Advanced Research in Biotechnology, National Institute of Standards and Technology, 9600 Gudelsky Drive, Rockville, Maryland 20850

Received June 7, 1995[⊗]

Abstract: The transphosphorylation step in the enzyme-catalyzed hydrolysis of phosphate esters by Ribonuclease A (RNase A) is explored using *ab initio* quantum chemical methods. For the first time, components found in the RNase A active site are included in the all-electron chemical model, made up of 2-hydroxyethyl methyl phosphate monoanion used as the substrate, and small model compounds used to mimic the three important residues, His-12, His-119, and Lys-41, found in the RNase A active site. The remainder of the immediate active site, including ten residues and six bound water molecules, is treated using effective fragment potentials (EFPs) incorporated directly into the Hamiltonian of the quantum system. The EFPs, derived from separate quantum calculations on individual components, are constructed to accurately represent the correct electrostatics and polarization fields of each component. High-resolution X-ray crystallographic data are used to assign the fixed relative positions of each component in the quantum and EFP regions. Characterization of the salient stationary points along the transphosphorylation reaction pathway at the RHF level using a 3-21+G(d) basis set reveals several low-barrier proton transfer steps between the substrate and the active site residues which allow transphosphorylation to occur with modest activation, consistent with the experimental data. Møller−Plesset perturbation theory (MP2) and density functional theory methods utilizing a larger 6-31+G(d) basis are also used to explore the effects of electron correlation on the surface energetics. Consistent with expectations, the electrostatic field effects from the EFPs used to represent the non-participating parts of the active site are found to differentially stabilize certain structures along the reaction pathway.

I. Introduction

Bovine Pancreatic Ribonuclease A (RNase A), a monomeric protein containing a single chain of 124 amino acid residues, is an efficient catalyst for the hydrolysis of phosphate−ester linkages in single-stranded RNA. For more than 50 years RNase A has been the focus of considerable research interest,[1] and thus is one of the most important prototype enzymes for the study of general protein function. Despite the progress made in elucidating features of the overall catalytic process, however, significant aspects of the RNase A microscopic mechanism remain unclear. The extent to which certain active site amino acid residues intimately participate in the enzymatic mechanism, and in what capacity, lies at the heart of the RNase A controversy. Ultimately, a more complete understanding of how RNase A functions will require a quantitative description of the individual microscopic steps which convert the reactant complex to the product complex (i.e. the microscopic enzymatic mechanism), a task not easily accomplished using direct experimental techniques alone.

The generally accepted mechanism by which RNase A functions to hydrolyze phosphate esters is the two-step general acid−base mechanism illustrated in Figure 1.[1c] The first step involves intramolecular transphosphorylation leading to a cyclic phosphate intermediate. In the subsequent step, the cyclic phosphate is hydrolyzed by a water molecule within the active site to form a monophosphate final product. Based on the available kinetic data, both steps in the reaction have comparable energies of activation, with k_{cat} ranging from 1 to 3000 s^{-1} depending on the nature of the substrate.[1] Based on simple transition state theory arguments, k_{cat}s which fall in this range correspond to activation free energies between 58 and 75 kJ mol^{-1}, nearly half that for the uncatalyzed reactions in solution at neutral pH.[2b] As shown in Figure 2, the transphosphorylation step involves in-line backside displacement at phosphorus through a pentacoordinate trigonal-bipyramid (TBP) structure, believed to be an important intermediate or transition state structure along the reaction pathway. Three residues within the active site of RNase A, His-12, His-119, and Lys-41, have been identified as the critical residues in the catalytic machinery. His-12 and His-119 are thought to act as the general base and general acid, respectively, in the first step of the mechanism, and are

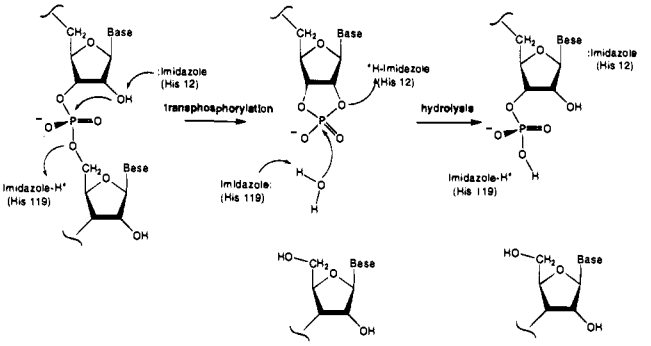

Figure 1. Schematic representation of the proposed overall phosphate−ester hydrolysis mechanism catalyzed by RNase A.

† National Research Council (NRC) Postdoctoral Fellow.

[⊗] Abstract published in *Advance ACS Abstracts,* October 1, 1995.

(1) For reviews see: (a) Richards, F. M.; Wyckoff, H. W. IN *The Enzymes*; Boyer, P. D., Ed.; Academic Press: New York, 1971; Vol. 4. (b) Blackburn, P.; Moore, S. *The Enzymes*; Boyer, P. D., Ed.; Academic Press: New York, 1982; Vol. 15. (c) Fersht, A. *Enzyme Structure and Mechanism*, 2nd ed.; W. H. Freeman and Co.: New York, 1985; pp 426−431.

(2) (a) Gerlt, J. A.; Gassman, P. G. *Biochemistry* **1993**, *32*, 11943. (b) Gerlt, J. A.; Gassman, P. G. Submitted for publication.

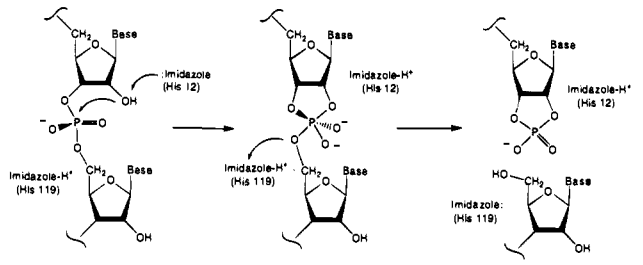

Figure 2. Schematic representation of the proposed mechanism for the transphosphorylation step in the RNase A enzymatic mechanism.

believed to reverse their roles in the second step. The specific role of Lys-41 remains unclear. It has been suggested that its primary function is to stabilize the presumed dianionic TBP structure through electrostatic interactions.[1] However, this hypothesis has never been confirmed.

Although the simplified mechanism described above and shown schematically in Figures 1 and 2 is consistent with most of the available experimental data on RNase A, a number of controveries regarding the specific details still remain. Recently, Breslow and co-workers[3] argued that the microscopic mechanism by which RNase A functions may be more complex. Using kinetic data from the hydrolysis of various dinucleotides by substituted β-cyclodextrins which act as enzyme mimics for RNase A they inferred that an initial proton transfer between His-119 and the anionic substrate takes place prior to deprotonation of the 2′-hydroxyl group in the transphosphorylation step. Moreover, structural data from high-resolution X-ray and neutron crystallographic studies of RNase A with a uridine vanidate bound in the active site[4] show that the imidazole ring of His-12 is not optimally positioned to fulfill its catalytic role in the proposed enzymatic mechanism. The catalytic nitrogen (Nδ1) of His-12 was found to lie closer to a non-bridging equatorial oxygen in the pentacoordinate oxy-vanidate compound than to the axial O2′ oxygen, as would be expected from the mechanism shown in Figure 2. Such structural information strongly suggests an alternative role, or at least a secondary role, for His-12.

In an attempt to resolve these and other issues in establishing a coherent picture for RNase A catalysis, aspects of phosphate–ester hydrolysis have been the subject of an increasing number of computational studies over the years.[5-8] Much of the initial theoretical work on RNase A and its enzymatic mechanism relied on classical mechanics[5] and focused primarily on the transphosphorylation step. In 1979 Holmes *et al.*[5a] developed the first molecular mechanics force fields for TBP phosphorane structures and applied them to the RNase A system. However, only the essential components of the active site were considered in this initial work in an attempt to confirm the basic transphosphorylation mechanism. In more recent theoretical work, Karplus *et al.*[7a-c,g,h] performed a series of molecular mechanics and dynamics simulations on a much larger fraction of the RNase A enzyme including a bound substrate and product complex. Key interactions between the substrate and residues within the active site were identified as a function of the protonation state. The results showed substantial movement of many active site side chains including both His-12 and His-119 depending on the protonation state, and these movements were found to be consistent with the proposed role of each residue.

Although classical-based methods can be useful to gain insight into many aspects of enzyme–substrate interactions, such methods are of little use in characterizing the discrete intermediates and transition states which lie along the enzyme-catalyzed reaction pathway. Characterization of the salient structures connecting the reactant and product complexes (i.e. the microscopic mechanism) is central to a more complete understanding of how enzymes work, and represents the first step in predicting enzymatic reaction rates computationally. Moreover, like all chemical transformations, reactions occurring within the confines of an enzyme active site are inherently electronic in nature and, therefore, require an appropriate quantum mechanical description. This is true not only for bond formation and bond cleavage but also for charge transfer processes between the substrate and enzyme. Charge transfer, including simple proton transfer between parts of the enzyme active site and the substrate as the reaction proceeds, is a fundamental component in many enzymatic mechanisms. As a result, the parts of the enzyme which *intimately* participate in such charge transfer processes must be considered explicitly in quantum treatments in order to achieve a realistic picture for enzymatic catalysis.

Due to practical time constraints and poor scalability, however, the use of more rigorous quantum techniques to compute properties of large chemical systems is far from routine. Much of the theoretical work to date in this area has focused on the use of hybrid quantum/classical methods for describing large chemical systems, especially those of biochemical interest. In recent review articles, Åqvist and Warshel[9] discussed the use of empirical valence bond (EVB) methods as a way to incorporate large parts of the environment in the study of enzyme-catalyzed and solvated reactions, while DeVries et al.[10] summarized the use of various reaction fields ranging in complexity from discrete distributed monopoles to continuum dielectrics. An alternative approach used in the computational study of large chemical systems quantum mechanically is based on the use of small model systems to emulate the essential chemical reaction of interest but with bulk environment left out entirely. A number of studies based on this latter approach relating to phosphate–ester hydrolysis have appeared recently in the literature.[6,7d-f,8] most of which focus on isolated oxyphosphorane structures and their relevance to the overall phosphate–ester hydrolysis mechanism. Lim and Tole[7f] were the first to characterize the complete transphosphorylation mechanism for a simple model substrate using *ab initio* methods. The gas-phase transphosphorylation reaction pathway for 2-hydroxyethyl methyl phosphate ester was determined at the RHF

(3) For a review see: Breslow, R. *Acc. Chem. Res.* **1991**, *24*, 317.

(4) (a) Ladner, J. E.; Wladkowski, B. D.; Svensson, L. A.; Sjolin, L.; Gilliland, G. L. *Biochemistry*. Submitted for publication. (b) Wlodawer, A.; Miller, M.; Sjolin, L. *Proc. Natl. Acad. Sci. U.S.A.* **1983**, *80*, 3628. (c) Borah, B.; Chen, C.; Egan, W.; Miller, M.; Wlodawer, A.; Cohen, J. S. *Biochemistry* **1985**, *24*, 2058.

(5) (a) Homes, R. R.; Deiters, J. A.; Gallucci, J. C. *J. Am. Chem. Soc.* **1978**, *100*, 7393. (b) Deakyne, C. A.; Allen, L. C. *J. Am. Chem. Soc.* **1979**, *101*, 3951. (c) Umeyama, H.; Nakagawa, S.; Fujii, T. *Chem. Pharm. Bull.* **1979**, *27*, 974.

(6) (a) Taira, K.; Uebayasi, M.; Maeda, H.; Furukawa, K. *Protein Eng.* **1990**, *3*, 691. (b) Uchimaru, T.; Tanabe, K.; Nishikawa, S.; Taira, K. *J. Am. Chem. Soc.* **1991**, *113*, 4351. (c) Taira, K.; Uchimaru, T.; Tanabe, K.; Uebayasi, M.; Nishikawa, S. *Nucl. Acid Res.* **1991**, *10*, 2747. (d) Storer, J. W.; Uchimaru, T.; Tanabe, K.; Uebayasi, M.; Nishikawa, S.; Taira, K. *J. Am. Chem. Soc.* **1991**, *113*, 5216. (e) Yliniemela, A.; Uchimaru, T.; Tanabe, K.; Taira, K. *J. Am. Chem. Soc.* **1993**, *115*, 3032.

(7) (a) Haydock, K.; Lim, C.; Brunger, A. T.; Karplus, M. *J. Am. Chem. Soc.* **1990**, *112*, 3826. (b) Lim, C.; Karplus, M. *J. Am. Chem. Soc.* **1990**, *112*, 5872. (c) Dejaegere, A.; Lim, C.; Karplus, M. *J. Am. Chem. Soc.* **1991**, *113*, 4353. (d) Lim, C.; Tole, P. *J. Phys. Chem.* **1992**, *96*, 5217. (e) Lim, C.; Tole, P. *J. Phys. Chem.* **1992**, *97*, 6212. (f) Lim, C.; Tole, P. *J. Am. Chem. Soc.* **1992**, *114*, 7245. (g) Dejaegere, A.; Karplus, M. *J. Am. Chem. Soc.* **1993**, *115*, 5316. (h) Dejaegere, A.; Liang, X.; Karplus, M. *J. Chem. Soc., Faraday Trans.* **1994**, *90*, 1.

(8) Krauss, M.; Basch, H. *J. Am. Chem. Soc.* **1992**, *114*, 3630.

(9) Åqvist, J.; Warshel, A. *Chem. Rev.* **1993**, *93*, 2523.

(10) De Vries, A. H.; Van Duijnen, P. Th.; Juffer, A. H.; Cullmann, J. A. C.; Dijkman, J. P.; Merenga, H.; Thole, B. T. *J. Comp. Chem.* **1995**, *16*, 37.

level using a 3-21+G(d) basis set. The theoretically-predicted stationary structures along the gas-phase reaction pathway were then used to formulate a detailed enzymatic mechanism for RNase A, including a description of the role for the three important active site residues. The work by Lim and Tole represents one of the first attempts to characterize the important structures along an enzyme-catalyzed reaction pathway using *ab initio* quantum chemical methods and represents an excellent first step toward a quantitative description of the true transphosphorylation reaction pathway. However, if the RNase A microscopic mechanism is to be modeled quantitatively using *ab initio* techniques, components of the enzyme active site which *intimately participate* in the reaction must be directly included in the analysis. We believe such considerations are critical to a more thorough understanding of enzyme-catalyzed mechanisms in general and the RNase A mechanism in particular.

Recently, we introduced a minimal model of the RNase A active site and probed the microscopic transphosphorylation mechanism using *ab initio* quantum mechanical methods.[11] In the present investigation we expand on this earlier work and explore the effects of the RNase A active site environment on the *microscopic mechanism* and *relative energetics* for transphosphorylation using a more complete quantum chemical model which includes more realistic parts of the enzyme active site. Non-participating components of the RNase A active site, which can influence the reaction through electrostatics and polarization fields, are also accounted for through the use of effective fragment potentials (EFPs). Our primary goal in this study is to determine a detailed microscopic mechanism by which RNase A facilitates transphosphorylation and to determine what specific role critical residues play in the microscopic mechanism. More importantly, we view the work on RNase A as a starting point for the development of a general methodology for studying other enzyme-catalyzed reaction mechanisms computationally.

Section II contains a detailed description of the theoretical model, including the specific chemical system considered and the constraints imposed. This section also contains the details of the *ab initio* calculations and an overview of the EFP approach. In Section III, the computational results including the structural and energetic data are presented, along with the discussion including a comparison of the results presented here with the available experimental and theoretical data on the RNase A transphosphorylation mechanism. Finally, a summary of the findings is given in Section IV along with a discussion of possible limitations in the model.

II. Theoretical Model

The structural model used in this investigation to analyze the transphosphorylation step of the RNase A enzymatic mechanism computationally consists of two major components, an all-electron quantum region and an effective fragment potential (EFP) spectator region. Together, these two regions account for a significant fraction of the entire enzyme active site. The quantum region contains a simple phosphate−ester substrate and the essential parts of the three most important amino acid residues found in the RNase A active site. This region is treated using traditional *ab initio* methods including Hartree−Fock, second-order Møller−Plesset perturbation theory (MP2), and density functional theory (DFT). The EFP spectator region contains all other non-participating components within the immediate first shell of the RNase A active site including ten complete amino acid residues and six bound water molecules found within an 8-Å sphere of the active site center as determined crystallographically. Each of the components in the EFP region is represented using a set of potentials which accurately describe their electrostatic and polarization fields. The appropriate potentials associated with each component are in turn derived from separate *ab initio* quantum calculations on the isolated species and can be incorporated directly into the one-electron Hamiltonian of the quantum region.

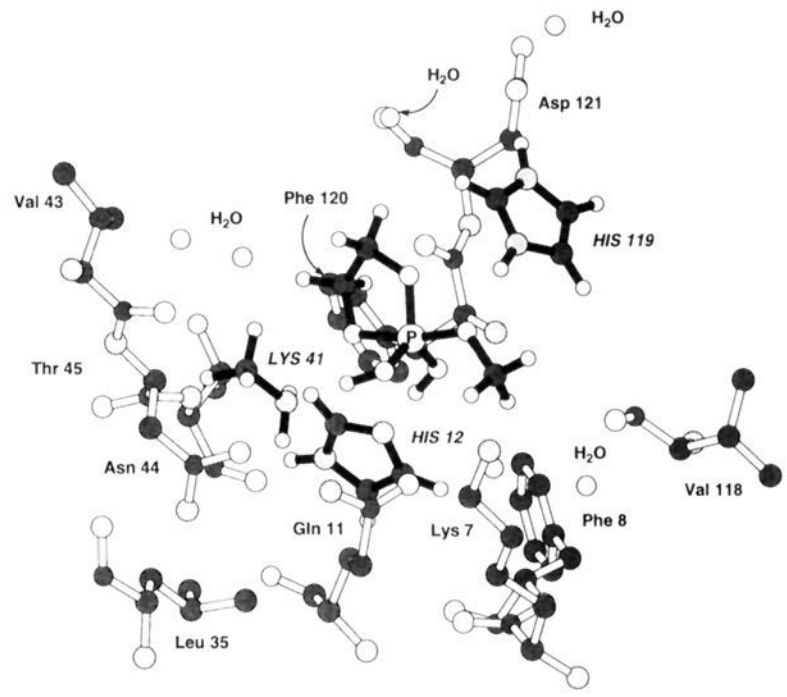

Figure 3. Three-dimensional representation of the complete chemical model used to study the RNase A transphosphorylation step including the all-electron quantum region (solid bonds) and the EFP spectator regions (open bonds).

A number of structural constraints must be imposed on both the quantum and EFP regions in order to construct a physically meaningful model which mimics the true RNase A active site environment. Unless the entire enzyme, or at least a significant fraction, is considered, such constraints are essential to prevent the movement of residues to unrealistic positions relative to the substrate. For this study, the coordinates from a recent high-resolution X-ray crystallographic study of a RNase A/uridine vanadate (RNase A/UV) complex[4a] are used to determine the appropriate relative constraints for each important residue in both the quantum and EFP regions. UV, a pentacoordinate oxyvanadium compound and a potent inhibitor of RNase A, binds as a non-reactive transition state or intermediate analog; the resultant X-ray crystal structure, therefore, represents an ideal reference system. Other crystal structures of native RNase A and of RNase A with various bound analogs are known and could have been used in this way; however, the latest RNase A/UV X-ray structure is one of the highest resolution structures available. Moreover, a comparison of available high-resolution crystal structures for the native enzyme as well as RNase A complexed with various analogs reveals little variation between the backbone and even the side chains within the active site. A three-dimensional representation of the RNase A/UV active site, obtained from the refinement of 1.3 Å resolution X-ray data, is given in Figure 3, and illustrates the relative position of all non-hydrogen atoms for each amino acid residue incorporated into the current structural model. Specific details regarding the actual constraints imposed on the quantum and EFP spectator regions utilizing the RNase A/UV structure are given below.

The overall procedure used here to probe the influence of the RNase A active site on the microscope mechanism for transphosphorylation can be summarized as follows: (a) Using standard *ab initio* quantum mechanical methods, the optimized structures and relative energetics of each stationary point along the transphosphorylation pathway involving the *quantum region* alone are determined; (b) the necessary EFPs for each individual nonparticipating active site component (amino acid residue and bound water molecules) are then computed *ab initio* at the fixed geometry found crystallographically; and (c) through single-point energy calculations with the EFPs including the effects of the combined EFPs on the quantum system are determined at each stationary point determined in part a.

Using the approach described above, the effects of the RNase A active site on the transphosphorylation reaction pathway and energetics can be probed at two different levels. First, the effects of the pseudoresidues included in the quantum region on the microscopic

(11) Wladkowski, B. D.; Krauss, M.; Stevens, W. J. *J. Phys. Chem.* **1995**, *99*, 6273.

transphosphorylation mechanism can be determined by direct comparison of the results from this study with previous computational results for the isolated phosphate−ester systems reported by Lim and Tole.[7f] Specifically, aspects of transphosphorylation which involve significant electron rearrangement between the pseudoresidues and the substrate, including proton transfers, can be considered rigorously. Secondly, the influence of electrostatic field effects from other non-participating residues in the RNase A active site on the relative energetics of transphosphorylation can then be gauged from the EFP contributions to the total energy without their explicit incorporation into the all-electron system. The use of EFPs in this way is ideal for the study of reactions occurring within the active site of an enzyme where directional field effects can be extremely important.

Effective Fragment Potential (EFP) Method. Incorporation of the electrostatic field effects from non-participating residues within the RNase A active site into the quantum system is based on the effective fragment potential (EFP) method. A complete description of the EFP approach, including its application to small chemical systems, can be found elsewhere.[12] Only a brief outline is presented here for clarity. The EFP method is based on a separation of the complete chemical system into two components, a quantum active region (AR) and an EFP spectator region (SR). The total Hamiltonian for such a system is defined as the sum of the AR and SR Hamiltonians plus an interaction term, V_{AR-SR}.

$$H' = H_{AR} + H_{SR} + V_{AR-SR} \tag{1}$$

The AR is treated using traditional *ab initio* quantum methods while the wave function of the SR is replaced by effective potentials which simulate the effect of the SR on the AR wave function through the interaction term V_{AR-SR}. Because the true wave function of the SR is replaced by potentials and the internal structure of the SR is held fixed, the SR Hamiltonian, H_{SR}, and its contribution to the total energy are constant and can be ignored. The EFPs for each fragment in the SR can be divided into three types:

$$V^{efp}_{AR\text{-}SR} = \sum_{k}^{K} V_k^{Elec} + \sum_{l}^{L} V_l^{Pol} + \sum_{m}^{M} V_m^{Ex\text{-}Rep} \tag{2}$$

where K, L, and M in eq 2 are the total number of reference points associated with each component in the potential. The first term in eq 2, V^{Elec}, represents the electrostatic potential of each fragment in the SR and is based on the distributed multipole analysis (DMA) of Stone.[13] The DMA approach has been found to reproduce the electrostatic field of simple molecules using expansion points at the atom centers and bond midpoints. For this study, the multipole expansion was truncated at the quadrupole term. The second term in eq 2, V^{Pol}, represents the polarization or the change in the electrostatic potential induced by the quantum AR. The method for describing distributed polarizabilities found to be most suitable for the EFP method is that developed by Garmer and Stevens[14] in which the molecular polarizabilities are decomposed in terms of localized molecular orbital (LMO) contributions. Finally, the third term in eq 2 is repulsive and describes the exchange-repulsion between the AR and SR at close distances. Such repulsion terms can be modeled using a linear combination of Gaussian functions which contain coefficients that are optimized to reproduce the exact exchange repulsion energy. It should be made clear that the first two terms used to describe each EFP can be obtained directly from separate *ab initio* calculations on the individual SR components and are the only two terms used in the present investigation; the V^{Ex-Rep} term, which could be important if full structural optimization were carried out with the EFPs in place, is not considered in this study. A more complete description of the EFP approach including the exact form of each term in the potentials can be found elsewhere, along with applications to small molecular systems.[12]

(12) Jensen, J. H.; Day, P. N.; Gordon, M. S.; Basch, H.; Cohen, D.; Garmer, D. R.; Krauss, M.; Stevens, W. J. *Modeling the Hydrogen Bond*; Smith, D. A., Ed.; ACS Symp. Ser. 569; American Chemical Society: Washington, DC, 1994; pp 139−151.

(13) Stone, A. J. *Mol. Phys.* **1985**, *56*, 1985.

(14) Garmer, D. R.; Stevens, W. J. *J. Phys. Chem.* **1989**, *93*, 8263.

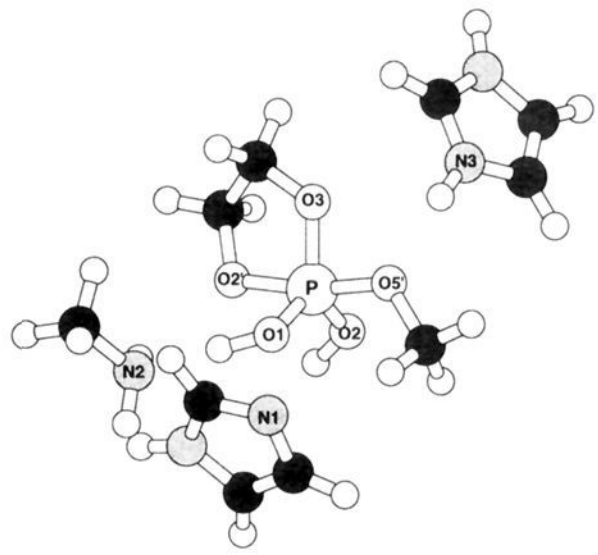

Figure 4. Three-dimensional representation of the diprotonated TBP phosphorane intermediate structure illustrating the components included in the quantum region, their relative orientation, and the important atom labeling.

Scheme 1

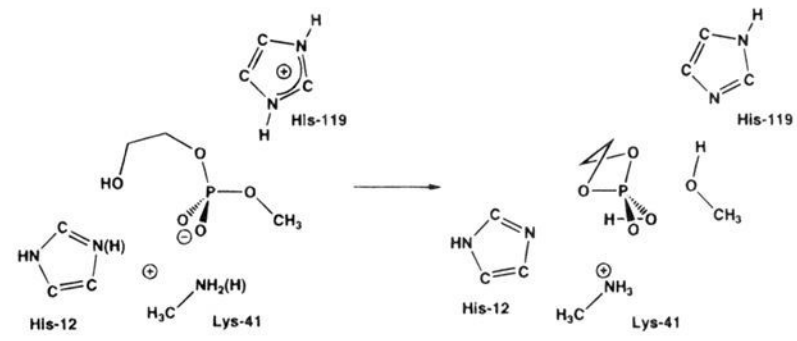

Quantum Active Region. Due to practical size limitations, the total number of atoms which can be included in the all-electron quantum region is fairly restricted. For this study, 2-hydroxyethyl methyl phosphate monoanion (HEMP) is chosen as the actual substrate. HEMP represents the smallest model of a complete phospho-dinucleotide with the essential features necessary to undergo intramolecular transphosphorylation. The products following transphosphorylation of HEMP are cyclic ethylene phosphate (EP) and methanol (Scheme 1). In addition to the substrate, critical parts of the three important active site residues, His-12, His-119, and Lys-41, are also included in the quantum region. These three residues are each represented by a small molecular subunit chosen to mimic the important features of each. Each histidine is represented by an imidazole ring, and Lys-41 is represented by a methylamine, CH_3NH_2. These "pseudoresidues" (hereafter written in italic to distinguish them from the complete residue) are chosen to allow for the necessary electron relaxation, including possible proton transfer between the active site components and the substrate, while maintaining a practical quantum region size allowing for an *ab initio* approach. The substrate HEMP, shown in Scheme 1 is the same substrate as that used by Lim and Tole[7f] in their initial study allowing for direct comparison with results for the isolated system.

The three pseudoresidues in the quantum region were held fixed in the same *relative* orientation as the corresponding subunits for each residue found crystallographically in the RNase A/UV complex discussed above. It is important to recognize, however, that no internal constraints were imposed on the pseudoresidues, only the relative orientation of each species was held fixed, and the substrate in the quantum region is unconstrained. As mentioned above, these relative constraints are necessary to maintain the proper three-dimensional arrangement of active site residues relative to the substrate and to one another, which in the actual enzyme is maintained by the rigidity of the protein backbone. The overall protonation state of the quantum system was chosen to mimic that expected experimentally based on available pK_a data, namely an anionic substrate, protonated Lys-41 residue, one protonated His, and one neutral His. This gives rise to an overall protonation state of +1 for the complete quantum system. Shown in Figure 4 is a three-dimensional representation of the most stable TBP phosphorane intermediate for transphosphorylation which illustrates the components included in the quantum system, their relative orientation, and the labeling scheme for the important atoms.

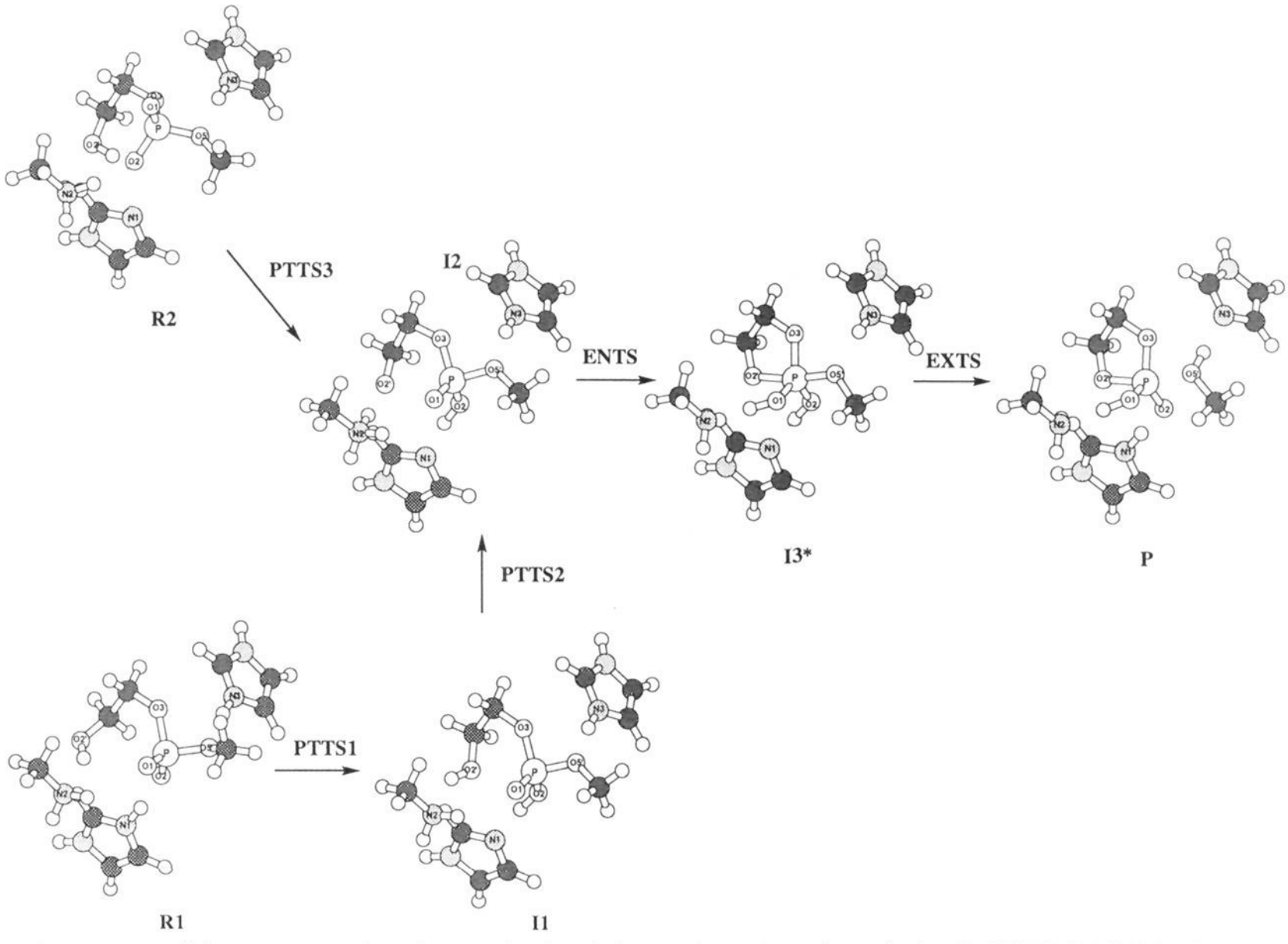

Figure 5. Important minimum structure along the transphosphorylation reaction pathway determined at the RHF 3-21+G(d) level (see text).

EFP Spectator Region. The EFP spectator region consists of all non-chemically-participating residues within an 8-Å sphere of the active site center. These residues include Lys-7, Phe-8, Gln-11, Leu-35, Val-43, Asn-44, Thr-45, Val-118, Phe-120, and Asp-121, as well as six bound water molecules, H_2O-333, H_2O-229, H_2O-294, H_2O-365, and H_2O-358 as determined directly from the X-ray crystal structure of RNase A/UV complex discussed above.

The EFPs for the complete spectator region were determined using the following procedure. First, the spectator region was separated into isolated unconnected groups of residues (7−8, 11, 35, 43−45, 118, 120−121, and each individual water). The heavy atom positions for each isolated group were taken directly from the RNase A/UV X-ray crystal structure and held fixed. Hydrogens were then added to each residue, including capping hydrogens for the C and N terminal ends of each segment, and assuming Lys-7 and Asp-121 are protonated and unprotonated, respectively, consistent with pK_a data. The hydrogen positions for the isolated fragments were then optimized at the RHF 3-21+G(d) level holding the heavy atoms fixed to their respective positions found crystallographically.[15] Using the final hydrogen-optimized structures, the electrostatic and polarization terms for each individual isolated group in the complete EFP spectator region were computed *ab initio* as outlined above. Together, the EFPs for the entire spectator region were used to estimate the effects of the active site environment on the quantum system via single-point energy calculations at each predetermined stationary structure of the all-electron quantum system. The position of the heavy atoms in each component of the EFP spectator region relative to the all-electron quantum region was also held fixed in the same orientation as that found crystallographically. A three-dimensional representation of the complete system including both the quantum and spectator regions is illustrated in Figure 3.

(15) The orientation of the hydrogens on the amino acid residues in the spectator region is dictated by the fixed position of the heavy atoms and can be determined unambiguously from the crystallographic data. The orientation of hydrogen on the water molecules cannot be determined unambiguously, but can be estimated from probable interactions with neighboring species.

Computational Details. The atomic orbital basis sets used in this investigation are the standard split-valence type generated by Pople and co-workers,[16] designated 3-21+G(d) and 6-31+G(d). The 3-21+G(d) and 6-31+G(d) basis sets consist of 247 and 449 contracted Gaussian functions, respectively, for the complete quantum region. Geometry optimization of the quantum region, as well as determination of the EFPs for each spectator residue, was accomplished using the smaller 3-21+G(d) basis set. The larger 6-31+G(d) basis set was used in subsequent single-point calculations at the associated stationary point on the surface. Reference electronic wave functions were determined by the single-reference, self-consistent-field, restricted Hartree−Fock method (RHF).[17] Dynamical electron correlation effects were accounted for using second-order Møller−Plesset perturbation theory[17] (MP2) and Density Functional theory (DFT) using the Becke exchange functional and Lee−Yang−Parr correlation functional (BLYP).[18−20] The core orbitals were excluded from the active space in all correlated calculations.

RHF analytic gradient techniques were used to determine the optimized structure of each stationary point along the reaction surface for the quantum region to 10^{-4} Å or rad in the internal coordinate space of each structure. Analytic second derivative calculations were used

(16) (a) Binkley, J. S.; Pople, J. A.; Hehre, W. J. *J. Am. Chem. Soc.* **1980**, *102*, 939. (b) Gordon, M. S.; Binkley, J. S.; Pople, J. A.; Pietro, W. J.; Hehre, W. J. *J. Am. Chem. Soc.* **1982**, *104*, 2797. (c) Pietro, W. J.; Francl, M. M.; Hehre, W. J.; Defrees, D. J.; Pople, J. A.; Binkley, J. S. *J. Am. Chem. Soc.* **1982**, *104*, 5039. (d) Hehre, W. J.; Ditchfield, R.; Pople, J. A. *J. Chem. Phys.* **1972**, *56*, 2257. (e) Hariharan, P. C.; Pople, J. A. *Theor. Chim. Acta* **1973**, *28*, 213. (f) Gordon, M. S. *Chem. Phys. Lett.* **1980**, *76*, 163. (g) Krishnan, R.; Binkley, J. S.; Seeger, R.; Pople, J. A. *J. Chem. Phys.* **1980**, *72*, 650. (h) Clark, T.; Chandrasekhar, J.; Spitznagel, G. W.; Schleyer, P. von R. *J. Comp. Chem.* **1983**, *4*, 294.

(17) Hehre, W. J.; Radom, L.; Schleyer, P. v. R.; Pople, J. A. *Ab Initio Molecular Orbital Theory*; Wiley-Interscience: New York, 1986, and references therein.

(18) Becke, A. D. *Phys. Rev. A* **1988**, *38*, 3098.

(19) Lee, C.; Yang, W.; Parr, R. G. *Phys. Rev. B* **1988**, *37*, 785.

(20) Miehlich, B.; Savin, A.; Stoll, H.; Preuss, H. *Chem. Phys. Lett.* **1989**, *157*, 200.

Table 1. Important Bond Distances (Å) for the Stationary Points Along the Transphosphorylation Reaction Pathway at the RHF 3-21+G* Level

stationary point	r(P−O2′)	r(P−O1)	r(P−O2)	r(P−O3′)	r(P−O5′)	r(N1−O2′)	r(N2−O2′)	r(N1−O2)	r(N2−O1)	r(N3−O5′)
R1	3.4870	1.4803	1.5100	1.6249	1.6243	3.7380	2.8563	2.6859	3.3031	2.7866
R2	3.3502	1.4762	1.5225	1.6228	1.6103	3.3957	2.7086	4.1050	4.6673	3.3295
I1	2.6266	1.4700	1.5609	1.5954	1.6129	3.1199	2.8471	2.7880	3.2159	2.7835
I2	2.7278	1.4814	1.5579	1.5857	1.6187	3.3648	2.7104	2.7007	3.0345	2.9553
I4*	1.7877	1.5646	1.5775	1.6276	1.6530	3.1199	2.9880	2.5897	2.6943	3.2287
PTTS1	2.6792	1.4763	1.5402	1.6174	1.6262	3.1402	2.8176	2.5527	3.1725	2.7574
PTTS2	2.7422	1.4745	1.5579	1.5886	1.6181	3.3248	2.6790	2.7239	3.1681	2.8268
PTTS3	2.9942	1.4764	1.5412	1.5872	1.6039	3.2497	2.7402	3.0400	3.6187	2.8890
ENTS	2.1435	1.5061	1.5715	1.6173	1.6452	3.2446	2.8134	2.6367	2.6876	3.2689
EXTS	1.7737	1.5775	1.5231	1.6170	1.7751	3.0696	3.0354	2.5369	3.1708	2.5647
P	1.7206	1.5619	1.5121	1.6094	1.8909	3.1210	2.9290	2.5296	2.7101	3.2096

Table 2. Relative Energetic Data (kJ mol^{-1}) for the Stationary Points Along the Transphosphorylation Reaction Pathway at Various Levels of Theory

stationary point	3-21+G*	6-31+G*			3-21+G*	
	RHF	RHF[a]	BLYP[a]	MP2(fc)[a]	EFP1[a,b]	EFP2[a-c]
R1	0.0	0.0	0.0	0.0	0.0	0.0
R2	38.5	6.3	13.0	7.9	40.6	45.2
I1	25.9	13.0	21.8	10.5	42.7	55.2
I2	55.6	74.5	52.7	44.4	66.9	61.9
I3*	45.6	39.3	32.2	6.7	44.4	50.6
PTTS1	36.4	54.0	31.4	26.8	50.2	56.9
PTTS2	77.0	120.9	70.7	74.5	85.8	87.4
PTTS3	94.1	91.2	66.1	66.1	98.7	97.9
ENTS	63.6	77.4	41.4	26.8	61.5	56.9
EXTS	97.9	120.5	70.3	53.1	110.5	76.1
P	68.6	61.5	46.9	24.7	134.7	63.2

[a] Single point calculations at the 3-21+G* RHF optimized structures. [b] EFP1 contains appropriate potentials for all ten residues plus six bound water molecules within an 8-Å sphere of the Rnase A active site center (see text). [c] EFP2 is identical to EFP1 except the potentials for Asp-121 have been removed.

to verify the character of each stationary point as a true minimum or transition state. Geometry optimization and subsequent MP2 and BLYP single-point calculations were performed using the GAUSSIAN 92 package,[21] whereas all calculations involving the use of EFP were carried out using the GAMESS[22] electronic structure package.

III. Results and Discussion

Optimized structures and related connectivities for each local minimum along the transphosphorylation reaction pathway as determined at the RHF 3-21+G(d) level for the isolated quantum region alone are given in Figure 5. More detailed structural information for each stationary point (local minima and transition states connecting them) is given in Table 1 for reference. The relative energetic data (ΔE^e_0, kJ mol^{-1}) for each stationary point as determined at various levels, with and without the EFP spectator region included, are listed in Table 2 and shown schematically in Figures 6−8. Figure 6 shows the relative energetic data at the RHF 3-21+G(d) level for transphosphorylation involving the quantum region alone. Figure 7 shows the effects of both basis set augmentation and electron correlation on the energetic data in Figure 6, while Figure 8 illustrates the influence of the EFP spectator region environment on the energetic data in Figure 6.

Reaction Coordinate. Fundamentally, the transphosphorylation step in the phosphate−ester hydrolysis reaction which

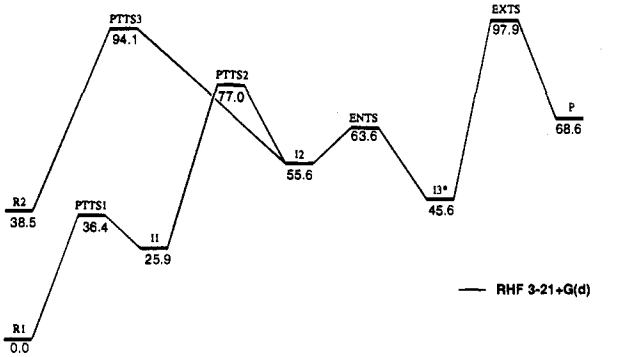

Figure 6. Relative energy diagram (kJ mol^{-1}) for the stationary points along the transphosphorylation pathway determined at the RHF 3-21+G(d) level.

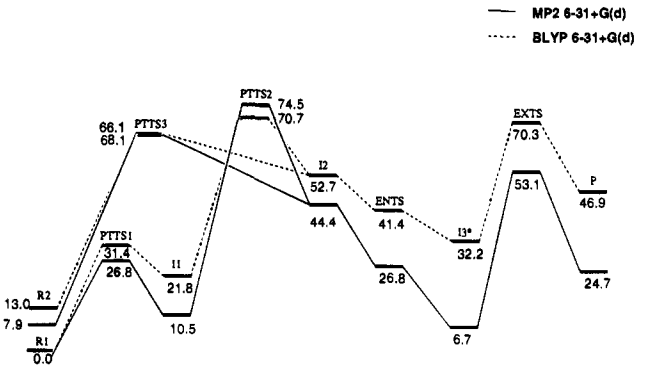

Figure 7. Relative energy diagram (kJ mol^{-1}) for the correlated single-point energy calculations at the predetermined stationary points along the transphosphorylation pathway given in Figure 5.

RNase A catalyzes is an intramolecular nucleophilic displacement at phosphorus by an activated alcohol in which the leaving group is also an alcohol. As expected, the qualitative reaction coordinate for intramolecular transphosphorylation shown in Figure 5 involves contraction of the O2′−P bond and an elongation of the O5′−P bond with inversion of the tetravalent phosphorus center. The values for these parameters change from approximately 3.4 and 1.6 Å, respectively, in the reactants, to approximately 1.7 and 1.9 Å, respectively, in the product complex (see Table 1). Although the general reaction can be considered simple nucleophilic displacement at a tetravalent phosphorus through a TBP structure, the overall reaction sequence must involve deprotonation of the nucleophile, and protonation of the leaving group. As a result, the overall reaction pathway contains a number of discrete intermediate states involving proton transfer between the *His-12*, *His-119*, and *Lys-41* pseudoresidues and the substrate. Interestingly, the most relevent TBP pentacoordinate structure found along the transphosphorylation reaction pathway is the diprotonated (neutral) intermediate phosphorane **I3***, and not a mono- or

(21) *Gaussian 92*, Revision A; Fisch, M. J.; Trucks, G. W.; Head-Gordon, M.; Gill, P. M. W.; Wong, M. W.; Foresman, J. B.; Johnson, B. G.; Schlegel, H. B.; Robb, M. A.; Replogle, E. S.; Gomperts, R.; Andres, J. L.; Raghavachari, K.; Binkley, J. S.; Gonzalez, C.; Martin, R. L.; Fox, D. J.; Defrees, D. J.; Baker, J.; Stewart, J. J. P.; Pople, J. A. Gaussian, Inc.: Pittsburgh, PA, 1992.

(22) Schmidt, M. W.; Baldrige, K. K.; Boatz, J. A.; Jensen, J. H.; Koseki, S.; Gordon, M. S.; Nguyen, K. A.; Windus, T. L.; Elbert, S. T. GAMESS. *QCPE Bull.* **1990**, *10*, 52.

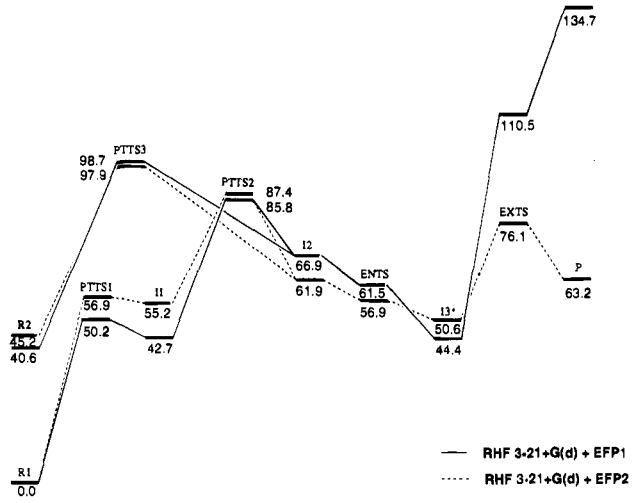

Figure 8. Relative energy diagram (kJ mol^{-1}) for the single-point energy calculations incorporating the EFP potentials at the predetermined stationary points along the transphosphorylation pathway given in Figure 5.

dianionic transition state as has been previously proposed. Starting from intermediate **I3***, the two pathways energetically accessible are exocyclic displacement toward products and endocyclic displacement back toward reactants. The exocyclic pathway through structure **EXTS** involves proton transfer between the *His-119* residue and O5′ of the substrate with concerted breakage of the O5′−P bond, consistent with previous proposals for the mechanism. **EXTS** leads directly to the product complex **P**, representing the association complex between methanol and protonated ethylene phosphate (EPH^+). Despite the formal breakage of the P−O5′ bond in the product complex, the P−O5′ distance is quite short, 1.89 Å, and suggests that there may be a considerable barrier for replacement of the alcohol product with a water molecule to initiate the second step in the overall hydrolysis reaction.

Alternatively, the endocyclic channel from intermediate **I3*** via elongation of the O2′−P bond from 1.79 to 2.73 Å through the endocyclic transition state structure **ENTS** leads to the intermediate structure **I2**. Structure **I2** can be formally considered an alkoxy phosphate anion in which charge has been transferred from the phosphoryl oxygen O1 to O2′. From the alkoxy structure **I2**, two energetically comparable pathways are possible, both of which lead to the reactant, HEMP. One pathway involves intramolecular proton transfer between the phosphoryl oxygen O2 and the alkoxy oxygen O2′, through **PTTS3**, leading directly to the reactant complex, **R2**. In the transition state structure **PTTS3**, *His-112* helps to facilitate the proton transfer but does not participate directly (i.e. the proton does not formally reside on N1). An alternative pathway from intermediate **I2** to the reactants involves initial proton transfer from the *Lys-41* catalytic nitrogen N2 to the alkoxy oxygen O2′ on the substrate through the transition state structure **PTTS2**, to form intermediate **I1**, followed by proton transfer from the phosphoryl oxygen O2 on the substrate back to *His-12* through structure **PTTS1**, leading to reactant structure **R1**. As can be seen in Figure 5, the only difference between reactant complexes **R1** and **R2** is the position of the proton. In structure **R1** the proton resides on *His-12*, whereas in structure **R2** it resides on *Lys-41*.[23] It is also interesting to note that throughout the reaction sequence, at each stationary point, the catalytic nitrogen on each of the three pseudoresidues His-12, Lys-41, and His-119, N1, N2, and N3, respectively, stays within close hydrogen bonding distance (2.6−3.0 Å) with three out of the five oxygen atoms surrounding the phosphorus. As seen in Table 1, N1 stays in close contact with either O2 or O2′ (primarily O2), N2 stays in close contact with O1 and O2′, and N3 maintains a hydrogen bond with O5′ throughout. This strongly suggests that all three residues are critical in the catalytic process. The qualitative features of the potential energy surface for transphosphorylation shown in Figure 5 are very similar to the results reported previously for the system in which methyleneimines (CH_2NH) were used instead of full imidazole rings.[11] The primary difference between the two systems is that a monoanionic TBP phosphorane structure was found to be a stable intermediate in the earlier work, whereas no such structures were found for the system described here.

Energetics. Considering the relative energetic data for the transphosphorylation reaction of the isolated quantum region alone shown schematically in Figure 6, a number of important results become immediately apparent. (1) The overall activation energy (ΔE^e_0) calculated at the RHF 3-21+G(d) level for the model transphosphorylation reaction is less than 105 kJ mol^{-1}, and considerably lower than estimates based on transphosphorylation of the substrate alone at the same level of theory as determined by Lim and Tole.[7f] These results clearly illustrate that the pseudoresidues included in the quantum region play a critical role in lowering the activation barrier by providing sites of moderate proton affinity, to and from which protons can be moved. (2) There exist a number of intermediate states along the reaction pathway which are associated with movement of protons between the substrate and the pseudoresidues, including the diprotonated TBP phosphorane structures, **I3***, which is found to lie approximately 46 kJ mol^{-1} above reactants at the 3-21+G(d) RHF level. (3) The most stable initial reactant state, **R1**, has the proton on *His-12* and not *Lys-41*, at variance with pK_a expectations.[24] Each initial reactant state, however, can lead to endothermic product formation through different channels of comparable energy, **PTTS2** or **PTTS3**. This suggests that *Lys-41* can play an intimate role in the catalytic process (i.e. general base) as opposed to simply stabilizing the intermediate phosphorane as has been proposed. In fact, the reaction channel starting from **R1** is found to be the overall lowest energy channel at the 3-21+G(d) RHF level. (4) Finally, an important feature of transphosphorylation identified in both reaction channels is *initial* protonation of a nonbridging phosphoryl oxygen on the substrate prior to nucleophilic attack at phosphorus. This is consistent with, but slightly different from, the mechanism proposed by Breslow,[3] in which His-119 is the initial protonating species.

The effects of electron correlation on the transphosphorylation potential energy surface energetics were estimated using second-order Møller−Plesset perturbation theory (MP2) as well as density functional methods employing the BLYP functionals. The relative energetic data from single-point MP2 6-31+G(d) and BLYP 6-31+G(d) calculations at the RHF 3-21+G(d) optimized stationary points (Figure 5) are shown schematically in Figure 7. Comparison of the data in Figure 7 with RHF

(23) It should be made clear that other possible orientations of the substrate within the pseudoactive site are possible which may give rise to a more stable arrangement. Structures **R1** and **R2** represent those relevant to the transphosphorylation reaction pathway.

(24) The pK_a ranges of Lys-41 and His-12 have been estimated to be 8.6−9.1 and 5.8−6.0, respectively, for the native enzyme without bound substrate. Therefore, protonated Lys-41 and unprotonated His-12 would be expected to be the most stable protonation states at neutral pH. In the gas phase, however, the reverse is true. The gas-phase proton affinity of imidazole (and methyleneimine) is greater than that of alkylamines (methylamine). Therefore, the relative stabilities of **R1** and **R2** are consistent with the limited model used here. To what extent desolvation of the enzyme active site shifts the results from a fully solvated pK_a representation to the gas-phase proton affinity ordering remains uncertain.

3-21+G(d) data in Figure 6 reveals a number of interesting trends. At the MP2 and BLYP levels, the energy of all points on the surface is reduced relative to the lowest energy structure which remains the reactant state **R1**. The relative energy of several structures is reduced substantially (42 kJ mol^{-1} or more). Interestingly, the largest shifts (RHF 3-21+G(d) to MP2 6-31+G(d)) are found for **ENTS** (36.8 kJ mol^{-1}), **I3*** (38.9 kJ mol^{-1}), **EXTS** (44.8 kJ mol^{-1}), and **P** (43.9 kJ mol^{-1}), the most product-like structures. Also, the relative energy of the endocyclic transition state, **ENTS**, is reduced much more than that of the intermediate, **I2**, at the MP2 6-31+G(d) level, indicating that these two structures may not be true stationary points at the higher level (i.e. the proton transfer transition state **PTTS2** and **PTTS3** may lead directly to intermediate **I3*** formation without activation). The relative energies of structures **PTTS3** and **EXTS** are reduced much more than that of **PTTS2**. As a consequence, the highest energy structure along the reaction pathway changes with the inclusion of electron correlation. As seen in Figure 7, **PTTS2** is now the bottleneck. This observation is also important because it indicates that although both reactant pathways are viable, the channel through **PTTS3** (intramolecular proton transfer) is favored at the highest MP2 level. The BLYP energetic data show the same general trends relative to the RHF surface as the MP2 results but to a lesser extent. For most points on the surface (except **PTTS2**), the BLYP relative energetic data fall between the RHF and MP2 data. Most importantly, the energetic features of the RHF and correlated surfaces are qualitatively similar, and the overall activation energy for transphosphorylation is well below 85 kJ mol^{-1}, consistent with expectations based on experimental kinetic data.

Finally, the EFP spectator region can be used to gauge the effects of the remaining residues in the immediate RNase A active site on the transphosphorylation potential energy surface. Shown schematically in Figure 8 are the results from the EFP single-point RHF 3-21+G(d) calculations performed at the predetermined RHF 3-21+G(d) stationary points for the quantum region alone. Designated RHF 3-21+G(d)+EFPx, each set of calculations incorporates the electrostatic and polarization potentials from the spectator region components directly into the quantum region Hamiltonian. Two different sets of EFP calculations were completed. In the first set, EFP1, the potentials from all residues in the EFP spectator region, including the ten residues and six bound water molecules found within the 8-Å sphere of the active site center discussed above, were included. The second set of single-point EFP calculations, EFP2, were identical to EFP1 except the potentials for one of the residues in the spectator region, Asp-121, were removed.

Comparison of the RHF 3-21+G(d) relative energetic data in Figure 6 for the transphosphorylation reaction involving the quantum region alone with the RHF 3-21+G(d)+EFP1 data in Figure 8 for which the complete spectator region potentials are included in the calculations shows significant differences, primarily in the product region of the potential energy surface. Most points on the potential energy surface exhibit shifts ranging from 2 to 16 kJ mol^{-1}; however, the product complex, **P**, is dramatically destabilized by nearly 67 kJ mol^{-1} at the RHF 3-21+G(d) level when the full set of EFPs are included. The relative energy of the exocyclic transition state, **EXTS**, is also destabilized in the presence of the full EFPs, but to a lesser extent. Clearly, the electrostatic and polarization terms used to describe the static environment of the RNase A active site region defined by the components in EFP1 are not conducive to the formation of the cyclic phosphate intermediate. In an attempt to probe the origin of this effect, a series of similar EFP calculations were performed in which parts of the EFP spectator region were systematically removed. From the analysis of the data it was discovered that the potentials associated with Asp-121, the only anionic residue in the active site region, produced the most significant changes in the potential energy surface. Included in Figure 8 are the relative energetic data from the single-point EFP calculations in which the Asp-121 potentials were excluded, EFP2. As seen in Figure 8, the relative energies of stationary points closest to the product region, including **P** and **EXTS**, are substantially reduced in the absence of the Asp-121 potentials, while the remainder of the surface is only moderately affected.

The dramatic effect of the Asp-121 residue potentials on the product region of the transphosphorylation potential energy surface is consistent with its location in the RNase A active site. As shown in Figure 3, Asp-121 is located proximate to the *His-119* pseudoresidue in the quantum region, on the opposite side of the imidazole ring from the O5′ oxygen of the substrate. In its position, the carboxylate group of Asp-121 can interact directly with Nϵ2 of *His-119* through an ionic salt bridge. Such an interaction would be expected to increase the proton affinity of the catalytic Nδ1 nitrogen on *His-119* (N3) through partial deprotonation of the imidazole ring. As seen in Figure 5, the last step in the formation of the cyclic phosphate product is protonation of the O5′ oxygen by the *His-119* pseudoresidue, and therefore, it is reasonable to expect the Asp-121 EFPs would destabilize this part of the transphosphorylation potential energy surface, since the role of His-119 is to act as a general acid. The question remains, why is Asp-121 positioned to interact with His-119 when its role in the transphosphorylation step is to act as a general acid? Given that His-119 must reverse its role in the second step of the reaction, the location of Asp-121 near His-119 is understandable. The results presented here seem to suggest that Asp-121 may in fact be mobile, moving into position next to His-119 only during the second step of the enzymatic reaction. It is also possible that Asp-121 may stay fixed, and the diminished efficiency in the first step is compensated in the second step. Despite the intriguing results given in Figure 8, one can only speculate about the role Asp-121 plays. Further studies in which Asp-121 is incorporated directly into the quantum region may be necessary in order to fully resolve this issue.

IV. Conclusion

In conclusion, two critical features of the RNase A active site environment (a general acid to neutralize the substrate and a general acid/general base pair to facilitate proton transfer) which promote transphosphorylation with modest activation have been identified. In the presence of a sufficient quantum environment to allow for a specific reaction pathway, the *intrinsic* barrier to transphosphorylation for the model system used here is found to be consistent with kinetic results for the actual RNase A enzyme. Viewed in this way, the function of RNase A is more than simply to mediate the corresponding gas-phase or solution-phase reaction through nonbonded interactions which stabilize the transition state. The key residues chemically participate through catalytic proton transfer giving rise to a microscopic mechanism that may be otherwise inaccessible. The concept of intimate interaction between active site residues within RNase A and the reacting system is certainly not new. Gerlt *et al.*[2] have argued the importance of strong hydrogen bond formation between groups with similar pK_a's as a way to help stabilize critical structures along the reaction pathway. Lim and Tole[7f] have also postulated intimate interactions between the substrate and active site residues and have even speculated

on specific roles for each residue in mediating the energetics of the anionic reaction they studied computationally.

The constraints of computer time and available *ab initio* methods have necessarily limited the RNase A model used to probe the mechanism. In order to fully evaluate the reliability and applicability of the theoretical approach used here to study the RNase A reaction mechanism, it is important to recognize some of the specific limitations in the current model, and how they may contribute to errors in the final analysis. Each of these limitations can be considered at two levels, those associated with omitting certain parts of the chemical system, and those relating to the model used to describe the parts which are included. Of these two types, the former are perhaps the most significant. In the present model, only components within an 8-Å sphere of the active site center are considered, no parts of the enzyme outside this region are accounted for. Many other residues in the protein, as well as bulk solvent surrounding the entire enzyme, may play an important role in catalysis. It has been suggested that long-range electrostatics effects due to highly polar or charged residues far removed from the active site can influence not only the energetics of the reaction but also the enzymatic mechanism itself in certain cases. Moreover, a description of bulk solvent may be important to account for dielectric effects on the electrostatic environment, particularly for residues on the surface of the protein, such as Asp-121, which can play a key role in catalysis.

In terms of the theoretical model itself, there are a number of improvements which may help to provide a more accurate description of the system, including adding flexibility to components in the EFP and quantum regions, and the incorporation of exchange-repulsion in the EFPs. Although most proteins are highly rigid, especially in the active site region, slight movements of important side chains throughout the enzymatic reaction may be necessary for optimum catalytic efficiency. In the current model, relative constraints are imposed to ensure the proper three-dimensional arrangement of residues relative to the substrate, and to prevent unrealistic movement of certain components in the quantum region. Plans for the future include expanding residue models out to the protein backbone and allowing movement of the side chains in the quantum region. Finally, a more elaborate *ab initio* description of the quantum region may be required to obtain highly accurate energetic results. Specifically, optimization of the quantum region using correlated wave functions would eliminate errors inherent in the single-point energy calculation approximation used in the current analysis. Correlated optimization of a system as large as the one consider here, however, is extremely computationally intensive and the advantages of such an approach are as of yet unknown.

Note Added in Proof: We view the computational results presented here on the transphosphorylation of a model phosphate ester by Ribonuclease A to be consistent with the kinetic data reported recently by Raines et al. (Messmore, J. M.; Fuchs, D. N.; Raines, R. T. *J. Am. Chem. Soc.* **1995**, *117*, 8057) using site-directed mutants of Ribonuclease A. Raines et al. found that site-directed mutants of Ribonuclease A, in which the active site residue, Lys-41, was replaced by a variety of functional groups, showed dramatically different catalytic efficiencies. It was concluded that Lys-41 intimately participates in the catalytic mechanism by donation of a hydrogen bond in the rate-limiting step.

Acknowledgment. We are grateful to Professor John Gerlt (University of Illinois, Urbana—Champaine) and Jan Jensen and Professor Mark Gordon (Iowa State University) for helpful discussion.

JA951847B